

## Vortex Motion Driven by a Background Vorticity Gradient

David A. Schecter and Daniel H. E. Dubin

*Physics Department, University of California at San Diego, La Jolla, California 92093*

(Received 7 May 1999)

The motion of self-trapped vortices on a background vorticity gradient is examined numerically and analytically. The vortices act to level the local background vorticity gradient. Conservation of momentum dictates that positive vortices (“clumps”) and negative vortices (“holes”) react oppositely: clumps move up the gradient, whereas holes move down the gradient. A linear analysis gives the trajectory of small clumps and holes that rotate against the local shear. Prograde clumps and holes are always nonlinear, and move along the gradient at a slower rate. This rate vanishes when the background shear is sufficiently large.

PACS numbers: 47.15.Ki, 47.32.Cc, 52.25.Wz

Self-trapped vortices can be clumps (vorticity excesses) or holes (vorticity deficits). The interaction of clumps and holes with a background vorticity gradient often plays an important role in 2D hydrodynamics. For example, the decay of 2D turbulence can be controlled by the slow drift of holes down a vorticity gradient [1]. The motion of hurricanes on a rotating planet is influenced by the north-south gradient in the Coriolis parameter, which can be thought of as a (potential) vorticity gradient [2–7].

Here, we calculate the rate at which clumps and holes ascend or descend a background vorticity gradient under the conditions that (i) the vortices are pointlike and (ii) the background flow has strong shear. While pointlike vortices and strong background shear may be rare in geophysical settings, they are common in nonneutral plasmas [1,8] and may also be found on planets, such as Jupiter, that have intense storms in strong zonal winds [9].

Clumps and holes can be classified as prograde or retrograde, depending on whether they rotate with or against the local background shear. We find that a linear analysis gives the motion of a retrograde vortex. Prograde vortices are always nonlinear and move at a slower rate that is given by a simple “mix-and-move” estimate.

We neglect viscosity and consider flows that are governed by the 2D Euler equations:

$$\frac{\partial \zeta}{\partial t} + \vec{v} \cdot \nabla \zeta = 0, \quad \vec{v} = \hat{z} \times \nabla \psi, \quad (1)$$

$$\nabla^2 \psi = \zeta.$$

Here,  $\vec{v}(r, \theta, t)$  is the velocity field,  $\zeta(r, \theta, t) \equiv \hat{z} \cdot \nabla \times \vec{v}$  is vorticity, and  $\psi(r, \theta, t)$  is a stream function. For analysis, the vorticity is decomposed into vortices ( $v$ ) and background ( $b$ ):  $\zeta = \zeta_b + \sum \zeta_v$ . We focus on the case where  $\zeta_b$  is positive, cylindrically symmetric, and monotonically decreasing at  $t = 0$ , making clumps retrograde and holes prograde.

Figure 1 shows that clumps ascend a background vorticity gradient, whereas holes descend the gradient [2,3]. At  $t = 0$ , a clump and a hole are placed in an axisymmetric background. The system is evolved with a vortex-in-cell (VIC) simulation that numerically integrates Eq. (1)

[10]. Eventually, the clump is driven to the peak in background vorticity, whereas the hole is driven toward the minimum. Such gradient-driven separation may help organize storms into bands of like-sign vortices on planets with strong zonal winds, with holes in vorticity troughs, and clumps on vorticity peaks [9].

The opposite drifts of clumps and holes can be understood by momentum conservation. A similar argument has been used to explain the motion of phase-space density clumps and holes in plasma turbulence [11]. We focus on cylindrical geometry, where the flow conserves canonical angular momentum,  $P_\theta \equiv \int d^2r \zeta r^2$ . The analysis carries over to planar geometry, where linear momentum replaces  $P_\theta$ .

When there is just one vortex,  $P_\theta$  consists of two parts, a background contribution and a vortex contribution:  $P_\theta = \Gamma_b \langle r^2 \rangle_b + \Gamma_v r_v^2$ . Here,  $\Gamma_b > 0$  is the total circulation of the background flow,  $\Gamma_v$  is the vortex circulation,  $r_v$  is the radial position of the vortex, and  $\langle r^2 \rangle_b$  denotes the  $\zeta_b$ -weighted spatial average of  $r^2$ . As indicated in Figs. 1 and 2, both clumps and holes mix and flatten the ( $\theta$ -averaged) background vorticity. As the background is leveled,  $\langle r^2 \rangle_b$  increases (since  $d\zeta_b/dr < 0$ ). To conserve  $P_\theta$ , a clump ( $\Gamma_v > 0$ ) must climb the background gradient and decrease  $r_v$ , whereas a hole ( $\Gamma_v < 0$ ) must descend the gradient and increase  $r_v$ .

We now determine the radial speed of the vortex. The vortex’s dominant translational motion is rotation

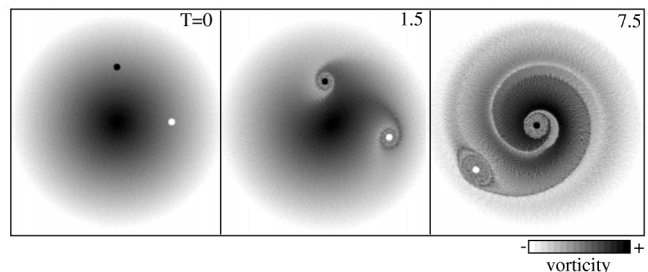


FIG. 1. Gradient-driven radial separation of a clump (black dot) and hole (white dot) in a circular shear flow.

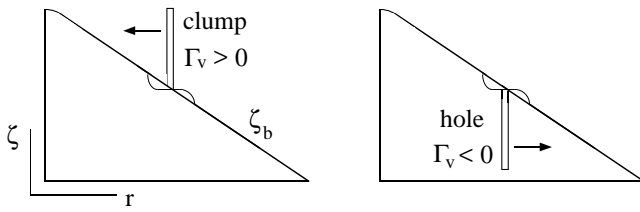


FIG. 2. Local mixing of the background increases  $\langle r^2 \rangle_b$ . By conservation of  $P_\theta$ , clumps and holes react oppositely.

about the center of the background. We work in this rotating frame, so the vortex is nearly stationary, and we define a local  $(x, y)$  coordinate system centered at the vortex. In these coordinates, the initial velocity due to the background is  $\vec{v} = Ay\hat{x}$  near the vortex, where  $A$  is the shear, and the initial background vorticity gradient is  $\zeta'_o \hat{y}$  (where  $\hat{y}$  points in the local  $r$  direction).

Figure 3 shows the initial streamlines in the vicinity of a retrograde clump [3(a)] and a prograde hole [3(b)]. The stagnation points in Fig. 3(a) are at a distance  $l$  above and below the clump, where

$$l \equiv \sqrt{|\Gamma_v/2\pi A|}. \quad (2)$$

We treat the vortex and the disturbance that it generates as perturbations to the initial shear flow, and suppose that the Euler equation for the evolution of  $\zeta_b$  can be linearized:

$$\left[ \frac{\partial}{\partial t} + Ay \frac{\partial}{\partial x} \right] \delta \zeta_b = -\zeta'_o \frac{\Gamma_v}{2\pi} \frac{x}{x^2 + y^2}. \quad (3)$$

Here,  $\delta \zeta_b$  is the background vorticity perturbation, and we have used  $\zeta_v = \Gamma_v \delta(\vec{x})$ . This assumes that the vortex is pointlike and moves slowly compared to the evolution of the background. We have also neglected the velocity perturbation due to  $\delta \zeta_b$ , assuming that it is negligible compared to the vortex velocity field.

Equation (3) can be solved by the method of characteristics, yielding

$$\delta \zeta_b = \frac{-\Gamma_v}{4\pi} \frac{\zeta'_o}{Ay} \ln \left[ \frac{x^2 + y^2}{(x - Ayt)^2 + y^2} \right]. \quad (4)$$

The radial velocity ( $\dot{r}_v$ ) of the vortex is the  $y$  component of the velocity perturbation that develops at the origin. By summing the contributions to the velocity field from each vorticity element, we obtain the following integral expression for  $\dot{r}_v$  (here,  $u \equiv x/y$ ):

$$\dot{r}_v = \frac{\Gamma_v}{4\pi^2} \frac{\zeta'_o}{A} \int_{-L}^L \frac{dy}{y} \times \int_{-\infty}^{\infty} du \frac{u}{u^2 + 1} \ln \left[ \frac{u^2 + 1}{(u - At)^2 + 1} \right]. \quad (5)$$

A small scale ( $l$ ) and a large scale ( $L$ ) cutoff are introduced to escape infinities in the  $y$  integral. The small scale cutoff describes the minimum distance from

the vortex at which nonlinearities in the background flow can be ignored. Thus, we identify the small scale cutoff with  $l$  [Eq. (2)], the size of the shaded trapping region in Fig. 3(a). To determine the upper cutoff, we note that curvature in the unperturbed flow cannot be ignored for  $|y| \gtrsim r_v$ , where  $r_v$  is the radial position of the vortex. We therefore set  $L = cr_v$ , where  $c$  is presumably  $O(1)$ .

The integrals in Eq. (5) yield

$$\begin{aligned} \dot{r}_v &= \frac{\Gamma_v}{2\pi} \frac{\zeta'_o}{|A|} \ln(L/l) \tan^{-1}(T/2) \\ &= \pm \zeta'_o l^2 \ln(cr_v/l) \tan^{-1}(T/2), \end{aligned} \quad (6)$$

where  $T \equiv |A|t$  and  $+/-$  is for clumps/holes. For  $T \gg 1$ , the inverse tangent is approximately  $\pi/2$ , and  $\dot{r}_v$  is approximately constant. Equation (6) gives a reasonable scaling for the vortex speed:  $\dot{r}_v$  increases with  $\Gamma_v$  and  $\zeta'_o$ , while it decreases as the local shear  $A$  intensifies.

However, the validity of Eq. (6) rests on the accuracy of Eq. (3), which neglects curvature in the unperturbed flow, the velocity perturbation due to  $\delta \zeta_b$ , motion of the vortex, and all nonlinear terms. We now test Eq. (6) against a VIC simulation that keeps all of these effects [10]. A linear simulation that incorporates the first three effects is used as an independent check.

We consider the specific case where the initial background vorticity distribution ( $\zeta_b$  at  $t = 0$ ) is given by

$$\zeta_o(r) = \begin{cases} 1 - 1.25 \cdot r & r \leq 0.8 \\ 0 & r > 0.8. \end{cases} \quad (7)$$

The rotation frequency of this background is  $\Omega_o(r) = 0.5 - 0.417 \cdot r$ , for  $r < 0.8$ . We assume that the flow is bounded by a circular wall with radius  $R_w = 1$ , and that there is free slip at the wall ( $\psi = 0$  at  $R_w$ ). The background chosen here represents a larger class, where the radial derivatives  $\zeta'_o$  and  $\Omega'_o$  vary slowly with  $r$ .

The linear simulation integrates the following set of equations. The vorticity perturbation is expanded as a Fourier series in the polar angle  $\theta$ :

$$\delta \zeta_b = \sum_{m=-\infty}^{\infty} Z^{(m)}(r, t) \cdot e^{im\theta}. \quad (8)$$

The linear evolution of  $Z^{(m)}$  is given by

$$\left[ \frac{\partial}{\partial t} + im\Omega_o(r) \right] \cdot Z^{(m)} = im \frac{\zeta'_o}{r} [\Psi_b^{(m)} + \Psi_v^{(m)}]. \quad (9)$$

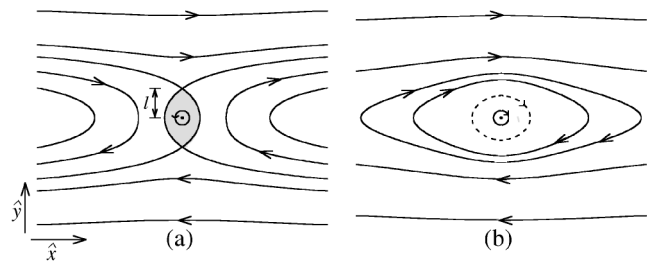


FIG. 3. Initial streamlines for a retrograde clump (a) and a prograde hole (b) in a shear flow  $\vec{v} = Ay\hat{x}$ ,  $A > 0$ .

Here,  $\Psi_v$  and  $\Psi_b$  are Fourier coefficients of the vortex stream function and the stream function of  $\delta\zeta_b$ . The vortex moves radially according to  $\dot{r}_v = -\partial\delta\psi_b/\partial\theta|_{\tilde{r}_v} r_v^{-1}$ , which can be written

$$\dot{r}_v = \frac{2}{r_v} \sum_{m=1}^{\infty} m \operatorname{Im}[\Psi_b^{(m)}(r_v, t) e^{im\theta_v}]. \quad (10)$$

The angular velocity of the vortex is given by the unperturbed flow,

$$\dot{\theta}_v = \Omega_o(r_v). \quad (11)$$

In the linear simulation, Poisson's equation is solved for  $\Psi_b^{(m)}$  to second-order accuracy in the radial grid-point spacing ( $\sim R_w/2000$ ). The vortex position  $\tilde{r}_v$  and the Fourier coefficients  $\{Z^{(m)}\}$  are evolved with third-order Adams-Bashforth steps ( $\sim 10^3$  steps per background rotation). The number of (excited) Fourier components is made finite in the linear simulation by setting  $\Psi_v^{(m)} = 0$  for  $m > \sqrt{e} r_v(t)/l(t)$ . This wave number is the inverse of the horizontal width (in radians) of the trapping region (TR) that is shaded in Fig. 3(a). Neglecting larger  $m$  amounts to neglecting the contribution to  $\dot{r}_v$  from the TR, where the fluid is rapidly ( $T \lesssim 1$ ) mixed by the vortex. Although the TR is defined only for a retrograde vortex, we try the same cutoff for a prograde vortex.

Figure 4 shows the linear (dashed line) and the VIC (solid line) computations of  $r_v(t)$  for a retrograde clump and a prograde hole of initial strength  $l/r_v = 0.12$ . The ratio  $l/r_v$  is called the ‘‘vortex strength’’ because it is a dimensionless measure of the vortex intensity relative to the background shear  $A = -r_v \Omega'_o(r_v)$ . The linear simulation of clump motion is in good agreement with the VIC simulation. In contrast, the hole moves much slower in the VIC simulation than in the linear simulation. The results for  $\theta_v(t)$  (not shown) give similar agreement for clumps and disagreement for holes.

Consider first the motion of the retrograde clump. It is apparent from Fig. 4 that the clump rapidly accelerates to a constant radial speed. Equation (6) offers a value for this speed, up to a factor  $c$  (of order 1) in the logarithm.

Rather than set  $c = 1$  on physical grounds, we use a precise value for  $c$  that can be obtained by a standard (but lengthy) analysis of Eqs. (9)–(11). Unlike the previous derivation of Eq. (6), this analysis incorporates curvature

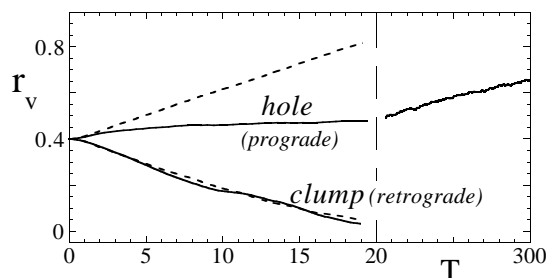


FIG. 4. Radial position of vortex versus time  $T = r_v(0)|\Omega'_o|t$  for linear (dashed) and VIC (solid) simulations.

of the unperturbed flow, and the velocity perturbation due to  $\delta\zeta_b$ . However, the calculation still makes use of an unperturbed orbit approximation:  $\delta\zeta_b$  is evolved with the vortex fixed on a circular orbit [ $\theta_v = \Omega_o(r_v)t$ ], and  $\dot{r}_v$  is taken to be the radial velocity perturbation at the vortex center. Wave numbers  $m > \sqrt{e} r_v/l$  are neglected, as in the linear simulation. The analysis yields a time-asymptotic value for  $\dot{r}_v$  that converges to Eq. (6) in the limit of small  $l/r_v$ . In general, the factor  $c$  depends on  $r_v$  and the form of  $\zeta_o(r)$ . In our example [Eq. (7)], the expression for  $\dot{r}_v$  reduces to Eq. (6) for  $l/r_v \lesssim 0.1$ , with  $c = 0.43$  for  $r_v \lesssim 0.7$ .

Figure 5 shows that the radial speed of the clump converges to linear theory [Eq. (6)] as the clump strength  $l/r_v$  approaches zero. All clumps start at  $r_v = 0.4$  and the background is always given by Eq. (7). We vary  $l/r_v$  by changing  $\Gamma_v$  only. We obtain  $\dot{r}_v$  from a straight-line fit to  $r_v$  vs  $t$ , as  $r_v$  decreases from 0.375 to 0.35. In the plot,  $\dot{r}_v$  is normalized to  $\zeta'_o r_v^2$ . Both  $\zeta'_o r_v^2$  and the clump strength  $l/r_v$  are evaluated at  $r_v = 0.363$ . The diamonds correspond to linear simulations and each ‘‘ $\times$ ’’ corresponds to a VIC simulation. The solid curve is the  $T \rightarrow \infty$  limit of Eq. (6), with  $c = 0.43$ . Both linear and VIC simulations converge to the solid curve as  $l/r_v$  tends to zero, indicating that the linear theory of Eq. (6) works well for retrograde vortices.

We now consider the motion of prograde holes. The failure of linear theory for holes can be understood by considering the streamlines in Fig. 3(b). Linear theory breaks down for times greater than the orbital period  $\tau$  of a fluid particle initially at  $x \sim l$ , the small length scale cutoff. The orbit of this particle is dashed. Since  $\tau \sim l^2/\Gamma_v$ ,  $\tau$  remains constant for holes as  $\Gamma_v$  approaches zero, while the time scale for the hole to move a distance of order  $l$  becomes infinite. Thus, the background perturbation around a small hole becomes nonlinear ‘‘instantaneously’’ for all practical considerations. For clumps [Fig. 3(a)], this problem does not arise, since fluid particles at  $x \geq l$  are not trapped around the vortex. Note that linear theory fails for holes, not because the hole has negative vorticity, but because the hole is prograde with respect to the shear flow in our example [Eq. (7)].

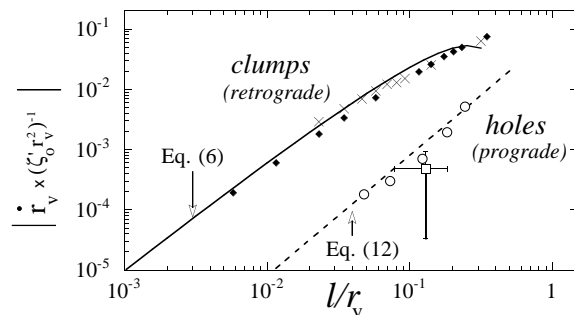


FIG. 5.  $\dot{r}_v$  versus  $l/r_v$  for linear simulation ( $\blacklozenge$ 's), VIC simulation ( $\times$ 's and  $\circ$ 's), and experiment ( $\square$ ).

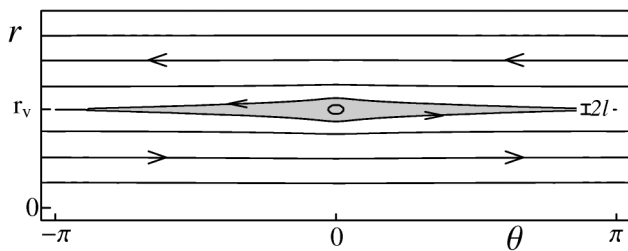


FIG. 6. Initial streamlines and mixing layer (shaded) for a prograde hole in a circular shear flow [Eq. (7)].

The following mix-and-move argument gives a good estimate for the hole velocity. A hole will attempt to mix a thin layer of background vorticity and move a distance  $\Delta r$  in response [Fig. 2(b)]. This mixing layer (ML) corresponds to the shaded region in Fig. 6, which shows the flow around a hole with  $l/r_v = 0.05$ . The ML extends from  $\theta = -\pi$  to  $\pi$  and has an average radial width of  $\sim 2l$ . Suppose that the hole levels the entire ML ( $\frac{d\langle \zeta_b \rangle_\theta}{dr} \rightarrow 0$ ) and has a negligible effect on fluid outside the ML. Then, using conservation of  $P_\theta$ , it can be shown that  $r_v$  must increase by  $\Delta r \sim l \zeta'_o / \Omega'_o$ . To obtain the hole velocity also requires an estimate of the time  $\Delta t$  required for the ML to flatten. The orbital speed of a trapped particle is on average dominated by the background shear, so  $\Delta t$  is approximately  $4\pi / l |\Omega'_o|$ . The velocity of the hole is  $\Delta r / \Delta t$ , or equivalently

$$\dot{r}_v \sim -\frac{1}{4\pi} l^2 \zeta'_o. \quad (12)$$

In Fig. 5, we compare Eq. (12) to the late time hole velocities that are observed in the VIC simulations. As before,  $\zeta_o$  is given by Eq. (7) and the holes are located initially at  $r_v = 0.4$ . The plotted values of  $\dot{r}_v$  are from straight-line fits to  $r_v$  vs  $t$ , as  $r_v$  increases from 0.5 to 0.6. The ratio  $l/r_v$  and the velocity normalization  $\zeta'_o r_v^2$  are evaluated at  $r_v = 0.55$ . The simulation velocities (denoted by  $\circ$ 's) are between 0.6 and 1.1 times the estimate, indicating that Eq. (12) is a reasonably accurate approximation for the speed of prograde vortices.

The speed of a prograde hole down a vorticity gradient was recently measured in an experiment [1]. The speed (plotted in Fig. 5) is within a factor of 4 of Eq. (12), which is at the level of estimated error. Although strong conclusions should not be drawn from a single datum, it appears that we have captured the basic mechanism for the radial motion of holes in the experiment.

The mix-and-move estimate assumes that the hole continuously moves into new regions where the  $\theta$ -averaged background vorticity has a slope  $\frac{d\langle \zeta_b \rangle_\theta}{dr} = \zeta'_o$ . However, if the ML moves with the hole,  $\frac{d\langle \zeta_b \rangle_\theta}{dr}$  shortly becomes zero at  $r_v$ , and the background and hole equilibrate in a phenomenon akin to the formation of a Bernstein-Greene-Kruskal

mode in a nonlinear plasma wave [12]. This will occur if  $\Delta t \ll t_l$ , where  $t_l$  is the time for  $r_v$  to increase by  $l$  and  $\Delta t$  is the mixing time. Using Eq. (12) for  $\dot{r}_v$  then implies that an equilibrium forms when  $\zeta'_o / \Omega'_o \ll 1$  [13].

For the simulation data in Fig. 5,  $\zeta'_o / \Omega'_o = 3$ , so only a small fraction of the ML moves with the hole [14]. However, by artificially increasing  $|\Omega'_o|$  in the VIC simulation so that  $\zeta'_o / \Omega'_o$  is less than 1, one can examine hole motion when the mix-and-move model breaks down. For  $\zeta'_o / \Omega'_o$  equal to 3/4 and 3/8 (and  $l/r_v = 0.2$ ), we find that the ML moves with the hole and an equilibrium is reached after a small radial displacement ( $\leq 0.1 r_v$ ).

Several issues remain. First, undamped modes or quasi-modes can affect vortex motion if their phase velocities resonate with the vortex velocity. This is particularly important when the background has steps [15]. Also, when  $l/r_v \geq 1$ , our linear treatment of retrograde vortex motion becomes invalid. Finally, our analysis indicates that there is a critical value of  $\zeta'_o / \Omega'_o$ , of order 1 for a prograde vortex and smaller for a retrograde vortex, below which equilibria form and above which the vortex continues to move. This nonlinear behavior merits further study.

The authors thank W. G. Flynn for his work on the VIC simulation and C. F. Driscoll for help with interpreting the experiment. This research was supported by NSF Grant No. PHY94-21318 and ONR Grant No. N00014-96-1-0239.

- [1] X. P. Huang, K. S. Fine, and C. F. Driscoll, Phys. Rev. Lett. **74**, 4424 (1995).
- [2] C. G. Rossby, J. Mater. Res. **7**, 175 (1948).
- [3] C. H. Liu and Lu Ting, Comput. Fluids **15**, 77 (1987).
- [4] G. F. Carnevale *et al.*, J. Fluid Mech. **233**, 119 (1991).
- [5] G. M. Reznik, J. Fluid Mech. **240**, 405 (1992).
- [6] R. K. Smith, in *Tropical Cyclone Disasters*, edited by M. J. Lighthill *et al.* (Peking University Press, Beijing, 1993), p. 264.
- [7] G. G. Sutyurin and G. R. Flierl, J. Atmos. Sci. **51**, 773 (1994).
- [8] K. S. Fine *et al.*, Phys. Rev. Lett. **75**, 3277 (1995).
- [9] For data, see Reta Beebe, Chaos **4**, 113 (1994).
- [10] D. A. Schecter *et al.*, Phys. Fluids **11**, 905 (1999). Here, we use at most  $1025 \times 1025$  grid points and  $3 \times 10^6$  particles.
- [11] T. H. Dupree, Phys. Fluids **26**, 2460 (1983).
- [12] I. B. Bernstein, J. M. Greene, and M. D. Kruskal, Phys. Rev. **108**, 546 (1957).
- [13] Similarly, we estimate that an equilibrium forms for a retrograde clump if  $2\pi^2 \sqrt{\ln(r_v/l)} \zeta'_o / \Omega'_o \ll 1$ , a substantially more stringent requirement when  $l \ll r_v$ .
- [14] In the experiment,  $\zeta'_o / \Omega'_o \sim 2-7$ .
- [15] I. M. Lansky, T. M. O'Neil, and D. A. Schecter, Phys. Rev. Lett. **79**, 1479 (1997).